

# Aerosol-Jet-Printed Silver Nanowires as Top Electrodes in Organic Photovoltaic Devices

Vanessa Arango-Marín,\* Juan S. Rocha-Ortiz, Tobias Osterrieder, Anastasia Barabash, Andres Osvet, Jonas Wortmann, Thomas Heumüller, Chao Liu, Jens Hauch, and Christoph J. Brabec\*

Aerosol jet printing (AJP) is an effective method for manufacturing organic photovoltaic (OPV) devices for indoor use. Its noncontact deposition, without posttreatment, and high-resolution 3D pattern printing capabilities make it ideal for using functional nanomaterial inks. This study explores ultrasonic AJP (uAJP) atomization to deposit silver nanowires (AgNW) as the top electrode layer (TEL) in OPV devices. The OPV stack is fabricated up to the hole transport layer using high-throughput screening (HTS) methodologies. Different deposition techniques, including spin-coating, blade-coating, and uAJP of AgNW inks, as well as thermal evaporation of silver, are compared. Scanning electron microscopy analysis shows that the E2X AgNW ink formed a compact TEL layer. Combining HTS setups, right selection of interlayers and uAJP method, automated, solution-processed OPV devices with power conversion efficiencies of 9.54% on an active layer of 0.0232 cm<sup>2</sup> are achieved, the highest reported for OPV devices using uAJP AgNW inks as top electrodes.

printing methodologies, such as inkjet printing (IJP) and aerosol jet printing (AJP) have been widely promoted in the contemporary landscape of OPV devices for indoor and outdoor applications. For instance, Maisch et al. showcased an IJP semitransparent OPV device employing AgNW as TEL.<sup>[1]</sup> However, this technology still faces significant challenges like tip clogging and limited resolutions. To overcome these obstacles, AJP, with higher resolution, smaller droplet sizes, and longer operation times before tip clogging occurs, has emerged as a novel alternative for depositing the layers on fully automated and solution-processed OPV production for indoor and outdoor applications.<sup>[1–3]</sup> Moreover, several studies have contributed to the solar energy landscape by reducing material consumption and research time

## 1. Introduction

The thermal evaporation method (Tevap) for deposition of top electrode layer (TEL) in organic photovoltaic (OPV) devices is widely used. However, its vacuum-associated costs are excessive. Moreover, spin-coating (SC) and blade-coating (BC) methods require postprocessing, incurring time, and cost. Therefore,


using high throughput screening (HTS) approaches.<sup>[4]</sup> Recently, the use of HTS on the charge transporting layers and photo absorber films in OPV fabrication was reported in our group.<sup>[5,6]</sup>

The hydrodynamic design inside the head of aerosol-jet (AJ) printers prevents tip-clogging issue because its surrounding sheath gas prevents the contact between the ink droplets and the tip walls.<sup>[7]</sup> Due to its direct-write 3D-CAD structuring, cost-effectiveness, and scalability, diverse researchers found AJP to be an excellent printing technique for ink deposition on optoelectronic devices.<sup>[8]</sup> In 2007, Mette et al. demonstrated ultrasonic AJP (uAJP) of silver ink as electrodes grids on silicon and not OPV devices.<sup>[9]</sup> Tu et al. utilized uAJP to pattern an AgNW ink onto transparent and flexible substrates in 2018.<sup>[10]</sup> Presently, studies in 2020 used the combination of PEDOT: PSS and AgNW but as a bottom electrode.<sup>[11]</sup> Hamjah et al. used pneumatic Aerosol Jet Printing (pAJP) for electrodes fabrication but over organic light-emitting diodes (OLED) in 2021,<sup>[11]</sup> and in the same year, Tam et al. employed AgNW as bottom and top electrodes reaching 3.73% power conversion efficiency (PCE) via BC. Finally, in 2022, Verboven et al. utilized uAJP to fabricate the anode on OLEDs,<sup>[12]</sup> and Tam et al. fabricated OPV devices by BC using Ag nanoparticle inks as electrodes and obtained 6.5% PCE.<sup>[13]</sup>

While earlier studies have proved the capabilities of AJP in fabricating electrodes and functional layers in context with 3D fabrication, there still is a need for further exploration of OPV devices with AJ-printed AgNW inks as TEL. Therefore, this study

V. Arango-Marín, J. S. Rocha-Ortiz, T. Osterrieder, J. Wortmann, T. Heumüller, C. Liu, J. Hauch, C. J. Brabec  
Forschungszentrum Jülich GmbH  
Helmholtz-Institute Erlangen-Nuremberg for Renewable Energies  
Gebäude HIERN-Immerwahrstr 2, 91058 Erlangen, Germany  
E-mail: vanessaarango@fau.de; christoph.brabec@fau.de

V. Arango-Marín, J. S. Rocha-Ortiz, T. Osterrieder, A. Barabash, A. Osvet, J. Wortmann, T. Heumüller, C. Liu, J. Hauch, C. J. Brabec  
Institute Materials for Electronics and Energy Technology  
Universität Erlangen-Nürnberg  
Martensstraße 7, 91058 Erlangen, Germany

 The ORCID identification number(s) for the author(s) of this article can be found under <https://doi.org/10.1002/solr.202400874>.

© 2025 The Author(s). Solar RRL published by Wiley-VCH GmbH. This is an open access article under the terms of the Creative Commons Attribution-NonCommercial-NoDerivs License, which permits use and distribution in any medium, provided the original work is properly cited, the use is non-commercial and no modifications or adaptations are made.

DOI: 10.1002/solr.202400874

aims to delve deeper into the use of AJP for the deposition as top electrode layers in OPV devices used in indoor and outdoor applications of next-generation photovoltaics. In this work, we used E2X AgNW ink as top electrodes using uAJP as deposition method to produce fully automated and solution-processed OPV devices. Moreover, we compared the PCE of the devices with uAJP, SC, BC AgNW inks, and Tenvap of Ag as top electrodes under different light intensities. Furthermore, we obtained the relationship between the printing passes parameter and their respective thicknesses on uAJP of AgNW inks as the TEL. Finally, we investigated the influence of the monolayer and bilayer on the hole transport layer (HTL) side to see its relation to the performance of the devices with SC, BC, and uAJP AgNW ink as top electrodes in OPV devices.

## 2. Results

Each device is prepared over a laser-patterned indium tin oxide (ITO) substrate with six different pixels or OPV cells conforming one device. For this purpose, we used the HTS setups, with the help of SPINBOT<sup>[5]</sup> and AMANDA-LineONE,<sup>[6]</sup> to process all the layers up to the HTL in an inverted structure using binary and ternary stable systems in the active layer. The devices were fabricated using similar methods explained in Osterrieder et al. work, where they developed an autonomous optimization in a 4-dimensional parameter space while SC the OPV devices with PM6:Y12:PC70BM as active layer.<sup>[6]</sup> In this study, we used the binary PM6:Y12 as active layer using the glass/ITO/ZnO/active-layer/BMHTL1 and glass/ITO/ZnO/active layer/BMHTL1/PH1000/ stacks. For the TEL, then we tried different deposition methods, such as, Tenvap, SC, BC, and AJP.

In AJP, the fine mist could be generated by different physical principles, such as atomization, evaporation/condensation, nebulization, or chemical reaction. The ultrasonic (uAJP) and pneumatic (pAJP) techniques use the atomization principle, in this case, atomization means that the liquid or ink will be broken down into small droplets inside a gas. In uAJP the ink is atomized using ultrasonic waves and in pAJP the atomization is generated by gas pressure. The pAJP is adept to deposit inks with high viscosity within the range of 1 to 1000 centipoise (cP), while uAJP is tailored to handle inks with lower viscosity, typically ranging from 1 to 5 cP.<sup>[8]</sup>

In uAJP, the ultrasonic waves generate high-frequency vibrations at the liquid–air interface, which leads to a cavitation effect that allows the formation and rapid collapse of microscopic bubbles at the liquid surface, when the bubble collapse it generates microjets and high-pressure zones at the surface, leading to the ejection of fine liquid droplets from the liquid–air interface. In pAJP, compressed inert gas pressure is used together with an atomizer that creates the shear forces and turbulence to atomize the ink.<sup>[14]</sup> The AJP working principles are illustrated in **Figure 1** uAJP system. Moreover, **Table 1** summarizes the good conditions found for uAJP of AgNW ink as top electrode layers in OPV devices with ITO/ZnO/PM6:Y12/BMHTL1/AgNW stack and ITO/ZnO/PM6:Y12/BMHTL1/PH1000/AgNW architecture.

We found decent printing parameters for uAJP of the ECOS HP 2X AgNW ink (E2X AgNW) obtained from HEIQ Materials AG. The E2X ink succeeded in creating uAJP electrodes on OPV device and to elucidate the reason behind it, we measured

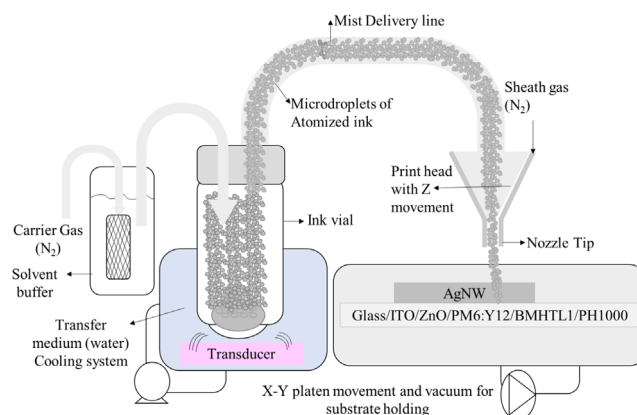


**Figure 1.** AJP working principles for AgNW ink deposition as the top electrode layer in inverted OPV devices the uAJP setup.

**Table 1.** AJP conditions for AgNW ink printing the top electrode layer in OPV devices using uAJP.

AJP conditions	Values
	uAJP
Tip type	3 mm
Sheath gas flow [sccm]	1000
Atomized gas flow [sccm]	500
Exhaust gas flow [cmm]	–
Initial ink volume [mL]	2
Initial solvent buffer [mL]	20
Platen temperature [°C]	30
Ink temperature [°C]	20
Atomization current [A]	0.18
Tip height [mm]	4
Printing speed [mm s <sup>−1</sup> ]	2
Printing passes [pp]	8
Filling type	Serpentine
Alternating printing [°]	0–90
Active layer system type	binary

the diameter and length of the nanowires on the E2X ink. Scanning electron microscopy (SEM) cross-sectional images of the E2X ink were acquired to provide insights into the length and diameter of the AgNW on the E2X ink. Figure S1, Supporting Information, presents examples of at least three SEM images used to obtain the statistics of the length and diameter of the nanowires in the E2X ink. To measure the diameters, we drop-casted 100  $\mu$ L of E2X ink over cleaned ITO substrates before uAJP treatment. Subsequently, top-view SEM images were acquired, and three images were employed to extract a minimum of 70 distinct diameter measurements. The average diameter of the nanowires on the E2X ink was  $49.36 \pm 9.2$  nm.

The lengths of AgNWs in the E2X ink were measured before and after 15 min of uAJP using 100  $\mu$ L aliquots from the ink. Notably, the initial AgNW length in the E2X ink was  $9.5 \pm 2.9$   $\mu$ m, which decreased to  $8.7 \pm 2.7$   $\mu$ m after uAJP

treatment, corresponding to a minor reduction of 8.1% from the original length. Thus, the uAJP conditions have a small impact on the AgNW length in the E2X ink, establishing it as a promising candidate for top electrode applications. Consequently, subsequent experiments focused on employing E2X AgNW ink in two distinct device stacks: ITO/ZnO/PM6:Y12/BMHTL1/TEL and ITO/ZnO/PM6:Y12/BMHTL1/PH1000/TEL, with either AgNW or Ag serving as the TEL in the OPV devices.

## 2.1. OPV Devices with a Monolayer HTL

Figure S2, Supporting Information, illustrates the characterization of E2X AgNW ink uAJP electrodes using top view and cross-section of SEM Images. Top-view images revealed that the electrodes exhibited a horizontal grid pattern, resulting from the specific slot-tip design utilized during aerosol jet printing process. Moreover, the thickness variation according to the number of printing passes of E2X of AgNW ink using uAJP as TEL over the ITO/ZnO/active layer/BMHTL1/stack is calculated measuring at least 70 thickness of the TEL on three different cross-section SEM images for the 7, 8, and 9 printing passes. The thickness of the TEL with 7, 8, and 9 pp of uAJP AgNW ink were  $336 \pm 46$ ,  $588 \pm 43$ , and  $589 \pm 34$  nm, respectively. As shown in the cross-sections of Figure S2, Supporting Information, the E2X AgNW ink formed a dense and rod-like layer of top electrode.

The first structure tried was the monolayer on the HTL and the ITO/ZnO/PM6:Y12/BMHTL1/TEL stack, the OPV device with uAJP AgNW ink was performed with the 3 mm tip on the ultrasonic aerosol jet printer. To compare the OPV devices performances, we used BC, SC, and uAJP for the E2X AgNW ink, as well as Tevap of Ag, as TEL over the stack. **Figure 2** represents the statistics of the  $J$ - $V$  parameters of the different OPV devices with the TEL performed with different deposition methods and under AM1.5 G illumination.

The PCE [%] average values of the OPV devices of at least two devices per deposition method under AM1.5 G of the organic solar cells (OSC) reference devices, with SC, BC, and uAJP the E2X AgNW ink, as well as Tevap of 100 nm Ag layer as a top electrode and using just one HTL on the HTL side were  $7.9 \pm 0.78$ ,  $8.1 \pm 0.89$ ,  $0.7 \pm 0.32$ , and  $11.3 \pm 0.89$ , respectively. The  $J$ - $V$  characterization results in Figure 2 show that the reference cells with Tevap Ag produce higher efficiencies than SC, BC, or uAJP AgNW inks as top electrodes. This finding aligns with the observations made by Tam et al., where they elucidated that the lower  $J_{sc}$  and fill factor (FF) on the devices resulted from the low reflectance and conductivity of AgNW compared with the Tevap Ag top electrodes.<sup>[15]</sup> Another reason for the lower performance of the SC, BC, and uAJP AgNW inks as TEL in OSC devices could be related to the s-shaped kink in their  $J$ - $V$  curves. These s-shaped curves were associated with a limited charge transport over the interfaces gathering space charges.<sup>[16]</sup>

The performance of the uAJP with the ITO/ZnO/PM6:Y12/BMHTL1/AgNW stack was relatively low because  $R_s$  values were extremely high, which probably explains the main part of the FF and  $J_{sc}$  losses, and it seems like there is a presence of a second diode, but that might be a mislead due to the very large  $R_s$ . The  $R_s$  values of the electrodes are in the order of magnitude acceptable for OPV application, however, the  $R_s$  values on the devices caused the high losses on the uAJP device performance. To conclude, the  $R_s$  value were probably interface limited and an alternative interface material needs to be screened, either to provide better film-forming properties or to provide lower contact resistance.

## 2.2. OPV Devices with Bilayer HTL

The crystallographic properties of AgNW have been extensively studied. Kalacha et al. (2022) analyzed the X-Ray diffraction patterns and presented high-resolution cross-sectional

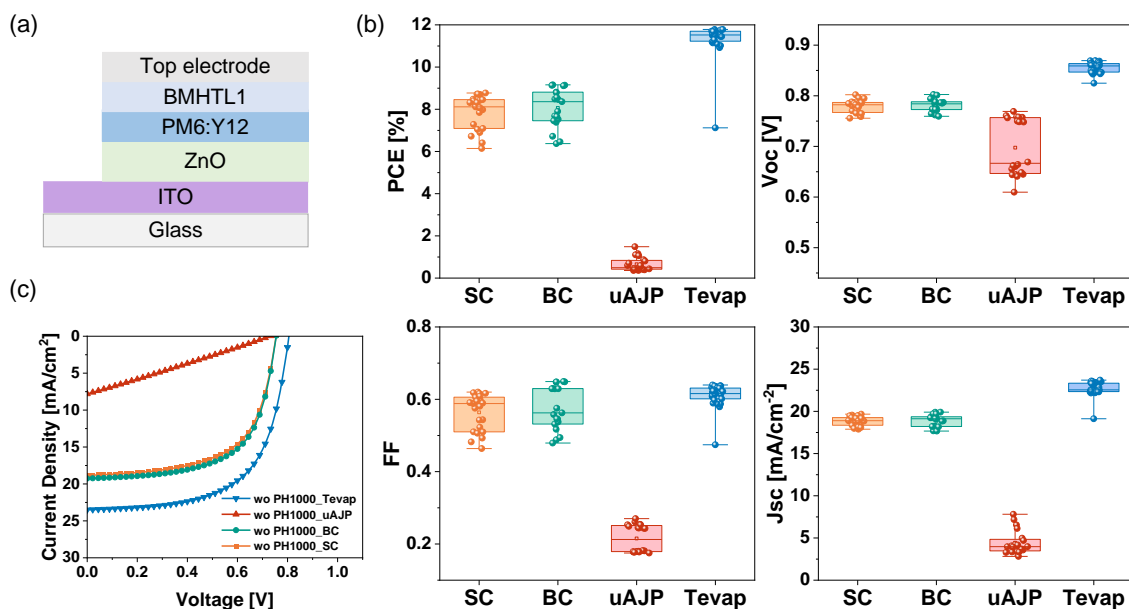


**Figure 2.** OPV devices a) structure without PH1000 b)  $J$ - $V$  parameters under AM1.5 G illumination of OPV devices: PCE,  $J_{sc}$ ,  $V_{oc}$ , and FF and c)  $J$ - $V$  curves of OPV devices with SC, BC, uAJP of E2X AgNW ink, and Tevap of Ag as TEL.

transmission electron microscopy images, revealing the characteristic fivefold twinned structure composed of five single-crystalline subunits.<sup>[17]</sup> Similarly, Schrenker et al. (2020) demonstrated this fivefold twinned crystal structure with a [110] growth direction, bounded by five [100] planes and capped by ten [111] planes.<sup>[18]</sup> The compositional properties of the E2X AgNW ink, specifically the concentration of Ag in isopropyl alcohol (IPA) was 1% or  $\approx 8 \text{ mg mL}^{-1}$ . We measured the transmittance over wavelength of the AgNW ink as electrodes thermally annealed at 130 °C for 5 min over glass/PH1000 substrates, as shown in **Figure 3**. Moreover, the  $R_{\text{sheet}}$  mean values were calculated by measuring the resistance of a 1 cm<sup>2</sup> electrode area twice on two different samples for each deposition method.

The optical properties of the E2X AgNW ink as top electrodes over glass/PH1000 substrates deposited using SC, BC, and uAJP methods are shown in **Table 2**. To elucidate the performance of the AgNW electrodes, the figure of merit (FoM) was calculated based on the transmittance at 550 nm and the sheet resistance of a 1 cm<sup>2</sup> square, following the formula described by Hackee.<sup>[19]</sup> The FoM values presented in Table 2 indicate that the highest-performing AgNW electrodes were fabricated using the SC deposition method, followed by those prepared with the uAJP and BC methods. The electrodes produced using the BC deposition method exhibited the lowest FoM values, which may provide insight into the lower efficiencies observed at the device scale for BC-based devices.

According to the results of monolayer HTL devices, we defined as the alternative interface material, the BMHTL1 and PH1000, both deposited by spin coating. Here, the ITO/ZnO/PM6:Y12/BMHTL1/PH1000/TEL stack was tried to improve the efficiency of the OPV devices. The *J*–*V* parameters of the different OPV devices are shown in **Figure 4**, where we used BC, SC and uAJP, for the E2X AgNW ink, as well as Tevap of Ag as TEL over the ITO/ZnO/PM6:Y12/BMHTL1/PH1000/ stack to compare its performances. The OPV devices with uAJP AgNW as top electrodes with this structure were performed with 3 mm tip and with 8 printing passes (pp) under the conditions shown in Table 1.

**Table 3** shows the statistics for the *J*–*V* parameters of the OPV devices with two HTLs. Moreover, Figure 4 shows the structure, *J*–*V* parameters, and curves of OPV devices with a bilayer on the HTL side under 1 sun light intensity. The efficiencies of the

**Table 2.** Transmittance, sheet resistance, and FoM of the AgNW electrodes over PH1000.

Deposition method	SC		BC		uAJP	
PH1000/AgNW	Mean	SD	Mean	SD	Mean	SD
Transmittance@550 nm [%]	84.1	2.55	88.0	0.62	72.8	0.08
Sheet resistance [ $\Omega/\square$ ]	24.9	3.37	280.0	0.82	29.0	0.14
FoM ( $T/R_{\text{sheet}}$ )	3.4	0.76	0.3	0.76	2.5	0.59

devices with SC and uAJP deposition methods were similar, while the devices with BC deposition method showed the lower efficiencies. On the devices with Tevap Ag as top electrodes, the one with the monolayer HTL presented better PCE performance than the reference device with the bilayer HTL due to the lower  $V_{\text{oc}}$  presented on the bilayer HTL devices. Moreover, employing the bilayer on the hole transport material side, we significantly improved the series resistance ( $R_s$ ) values of the OPV devices with uAJP AgNW ink as TEL, by decreasing them in around one order of magnitude, as observed in Figure S3, Supporting Information. The higher the  $R_s$  the lower the PCE performance of the devices in mono- and bilayer HTL. The data clearly demonstrate that, for structures incorporating PH1000, uAJP, and SC are more effective deposition methods for AgNW top electrodes compared to BC, primarily due to their lower  $R_p$  values.

Figure S4, Supporting Information, presents the *J*–*V* parameters of OPV devices with bilayer HTLs and AgNW inks as top electrodes, fabricated using SC, BC, and uAJP deposition methods, under both lower and higher light intensities compared to 1 sun. The performance of the devices followed trends similar to those observed under 1 sun illumination, with the uAJP and SC methods yielding comparable efficiencies, while the BC method exhibited lower efficiencies, primarily due to reduced parallel resistances,  $R_p$  or  $R_{\text{shunt}}$  values. The performance of the AJP devices under lower light intensities, such as 0.5 suns, was outstanding because the FF was higher. Interestingly, the  $R_p$  values of the devices with BC deposition method were lower than the  $R_p$  of the uAJP and SC devices, while the  $V_{\text{oc}}$  of AJP devices remained similar. Finally, the external quantum efficiency (EQE) and integrated  $J_{\text{sc}}$  over the wavelength in OPV devices with double HTL and different deposition methods for the TEL are shown in **Figure 5**.

The promising efficiencies of uAJP deposition method for depositing the AgNW ink as top electrodes in OPV devices is an encouraging result since uAJP offers several advantages for printing OPV devices, such as higher resolution, more environmentally friendly printing technique with less waste, lower production costs, and higher reliability.<sup>[20–24]</sup> In summary, this study demonstrates the feasibility of utilizing uAJP to deposit AgNW inks as top electrode layers in OPV devices suitable for both indoor and outdoor applications. By optimizing the device structure, the uAJP deposition method achieved higher PCE values compared to SC and BC. However, despite the incorporation of the PH1000 layer, the Tevap method consistently exhibited higher efficiencies than uAJP, albeit at the cost of significantly greater energy and time consumption.

Additionally, we showed that the performance of the devices with uAJP AgNW ink as top electrodes using stacks with a bilayer on the HTL side (BMHTL1/PH1000), was considerably higher

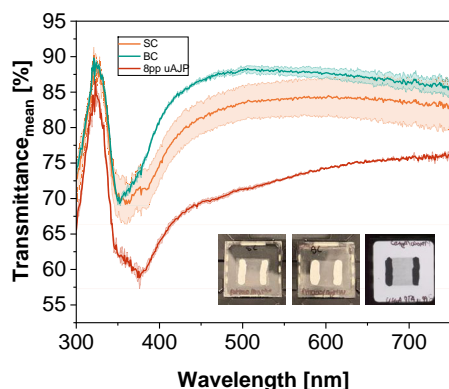


**Figure 3.** Optical transmittance spectra of the E2X AgNW ink deposited with different methods over wavelength; the inset shows examples of the photos of PH1000/AgNW electrodes of 1 cm<sup>2</sup> area deposited with SC, BC, and uAJP.

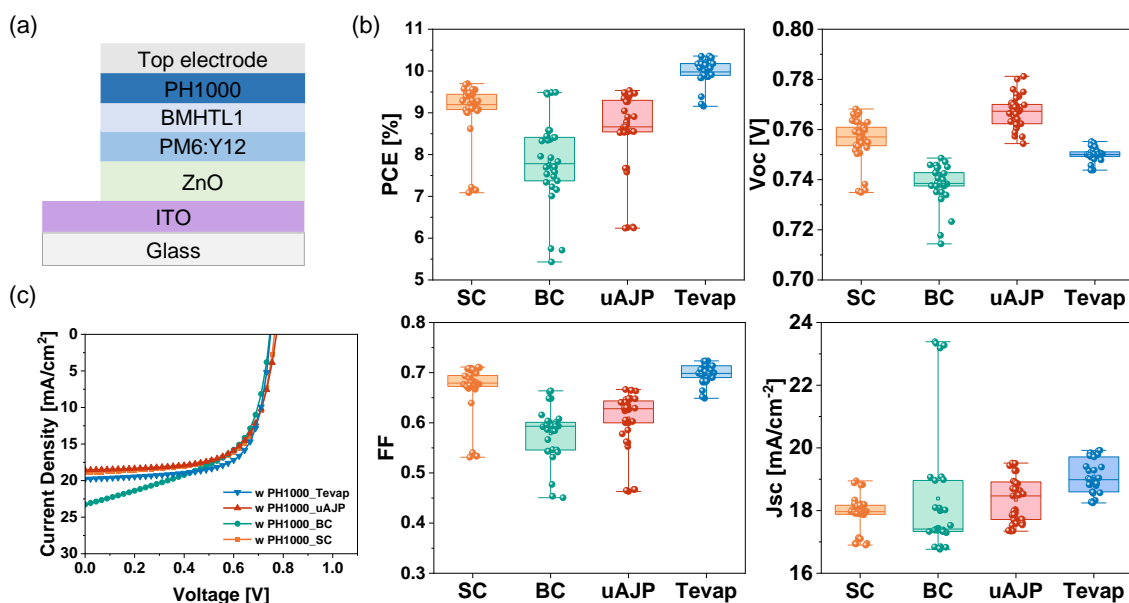


**Figure 4.** OPV devices a) structure without PH1000 b)  $J$ - $V$  parameters under AM1.5 G illumination of OPV devices: PCE,  $J_{sc}$ ,  $V_{oc}$ , and FF and c)  $J$ - $V$  curves of OPV devices with SC, BC, uAJP of E2X AgNW ink, and Tevap of Ag as TEL.

**Table 3.**  $J$ - $V$  parameters statistics of OPV devices with double HTL.

Deposition method	$J_{sc}$ [mA cm <sup>-2</sup> ]	$V_{oc}$ [V]	FF	PCE [%]
SC	17.9 ± 0.52 (18.95) <sup>a)</sup>	0.756 ± 0.0080 (0.768)	0.6695 ± 0.04730 (0.7112)	9.06 ± 0.671 (9.7)
BC	18.4 ± 2.03 (23.39)	0.738 ± 0.0078 (0.749)	0.5787 ± 0.05183 (0.6638)	7.85 ± 1.010 (9.49)
uAJP	18.4 ± 0.71 (19.51)	0.767 ± 0.0059 (0.781)	0.6085 ± 0.05577 (0.6665)	8.57 ± 0.922 (9.54)
Tevap	19.1 ± 0.53 (19.92)	0.750 ± 0.0025 (0.755)	0.6978 ± 0.01893 (0.7234)	9.99 ± 0.293 (10.36)

<sup>a)</sup> average value ± standard deviation (maximum value).

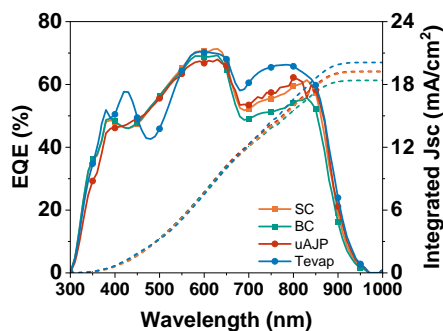


**Figure 5.** EQE and integrated  $J_{sc}$  over the wavelength in OPV devices with SC, BC, uAJP of E2X AgNW ink, as well as Tevap of Ag as TEL in OPV devices all with ITO/ZnO/PM6:Y12/BMHTL1/PH1000/Ag or AgNW structure.

than that of the monolayer HTL devices due to the high series resistance ( $R_s$ ) on the monolayer HTL devices. This might explain the biggest part of the losses in FF and  $J_{sc}$ . The architectures are still suffering from slightly large  $R_s$  values, which are limited by the interface conductivity value from the electrodes, therefore using a highly conductive second layer on the HTL side, the PH1000, was a successful approach to reduce the  $R_s$  and

produce better performances on the organic photovoltaic devices with ultrasonic aerosol-jet-printed silver nanowires as top electrode layer.

From the  $R_s$  and  $R_p$  inducing performance losses on the devices, we may conclude that the electrodes in the devices are still in the range of working electrodes for OPV devices. Moreover, the  $R_s$  was interface limited, ever since the performance of the OPV devices with AgNW ink as top electrode layer improved using a bilayer on the HTL side. The uAJP technique is useful for 3D printing electronics because it is a contactless and maskless printing method that could be used without the need for postprocessing layers, whereas the BC and SC techniques face limitations. This study demonstrates the feasibility of fabricating OPV devices using uAJP to deposit AgNW inks as top electrodes, achieving efficiencies comparable to or superior to those of OPV devices with AgNW top electrodes deposited via SC or BC.

### 3. Conclusion

In this study, we evaluated uAJP for depositing silver nanowire (AgNW) E2X ink as a top electrode layer in OSC devices.

We compared uAJP, SC, and BC AgNW inks as top electrodes in OPV devices. We found that while thermally evaporated silver (Tevap Ag) outperformed solution-based methods, it does not offer the advantages of uAJP in terms of 3D conformability and time-energy efficiency. By employing the E2X AgNW ink that stands the AJP conditions, and by developing a bilayer interface made from BMHTL1, which provided a good contact to the active layer, and PH1000, which provided a good contact to the electrode, we have been able to demonstrate OPV cells with a uAJP AgNW ink as top electrodes. The indoor and outdoor performance of devices with a bilayer HTL is not constrained by  $R_s$  values, unlike devices with a monolayer HTL. In this work, using the ITO/ZnO/PM6:Y12/BMHTL1/PH1000/AgNW stack and under 1 sun of light intensity we obtained the PCE average values of 9.06, 7.85, and 8.57% for SC, BC, and uAJP deposition methods, respectively. It can therefore be anticipated that uAJP is a suitable technology for printing top electrode layers using NW inks. However, further investigation is required to confirm its applicability with other types of inks, such as those based on alternative solvents or different metal-based nanowires.

## 4. Experimental Section

**Materials:** The ITO substrates were laser patterned to have six active layer spots or pixels or solar cells on each substrate or device. They were purchased from Liaoning Yike Precision New Energy Technology Co., Ltd. Additionally, we used the ZnO (N10) as ETL with Avantama AG concentration of 2.5% on IPA, sonicated for one minute, and passed through a 0.45  $\mu\text{m}$  polytetrafluoroethylene (PTFE) filter. All materials were used as received. PM6 was purchased from Solamer Materials, Y12 from T-material, PC70BM from Solenne BV, and BMHTL1 and PH1000 from Brilliant Matters and Heraeus Epurio, respectively. The IPA-based AgNW E2X ink had 1%Ag ink from HEIQ Materials AG.

**Equipment:** For blade coating, we utilized a ZAA 2300 Automatic Film Applicator Coater, with a ZUA2000 aluminum blade set at 400  $\mu\text{m}$  gap from Zehntner Testing Instruments, and for the uAJP of the AgNW inks, an AJ300 printer from Optomec was used. We used SPINBOT<sup>[5]</sup> and AMANDA LineOne<sup>[6]</sup> to obtain the  $J-V$  parameters and optical density (OD) of our OSC devices. We used the SEM JSM-7610 F from JEOL Ltd. to characterize the length and the diameter of the AgNW inks before and after uAJP. Moreover, we used a setup to measure  $J-V$  curves on each device in the dark and under AM1.5 G, employing a SINUS-70 solar simulator from Wavelabs and EQE measurements were performed with QE-R from Enlitech.

**Devices Preparation:** At least two devices per deposition method were measured. We consecutively cleaned the ITO/glass substrates with sonication for 10 min each on DIW, acetone, and IPA. Then, we used the SpinBOT to process the ZnO Avantama N10 as ETL using 60  $\mu\text{L}$ , 2500 rpm, and 200  $^{\circ}\text{C}$  of annealing temperature for 30 min under air. To produce the OPV devices we used LineONE<sup>[6]</sup> under nitrogen atmosphere. On the active layer, we utilized the PM6:Y12 system with a solid concentration of 19  $\text{mg mL}^{-1}$  at a ratio of 1:1.2 on *o*-xylene. The solution was magnetically stirred at 600 rpm overnight at 80  $^{\circ}\text{C}$ . Then, we SC the active layer using 25  $\mu\text{L}$  and 1100 rpm. On top of it, we spun 50  $\mu\text{L}$  of BMHTL1 as HTL at 3000 rpm for 60 s. The PH1000 layer was SC with 4000 rpm, 150  $\mu\text{L}$ , and for 60 s. Further, we either thermally evaporated Ag, SC, BC, or uAJP AgNW ink as the top electrode layer. For each type of ink, we SC with 600 rpm, 20 s, and 55  $\mu\text{L}$  and BC with 300  $\mu\text{m}$  gap, 20  $\text{mm s}^{-1}$ , 40  $^{\circ}\text{C}$ , and 60  $\mu\text{L}$ . Subsequently, for another type of reference cell device, instead of AgNW inks as top electrodes, we used 100 nm Ag. Finally, we compared those devices with the BC, SC, uAJP AgNW ink, and Tevap Ag as top electrodes based on OSC device performance. Finally, we uAJP the IPA-based E2X ink as top electrode with the conditions indicated in Table 1 and thermal annealed at 130  $^{\circ}\text{C}$  for 5 min under nitrogen.

## Supporting Information

Supporting Information is available from the Wiley Online Library or from the author.

## Acknowledgements

V.A.M. would like to thank the Ministerio de Ciencia, tecnología e Innovación de Colombia, for the DoctoradoExterior-885 Grant. J.S.R.O., V.A.M., J.H., and C.J.B. gratefully acknowledge financial support from the Helmholtz Association in the framework of the innovation platform “Solar TAP”. C.J.B. and J.H. gratefully acknowledge grants “ELF-PV”-Design and development of solution-processed functional materials for the next generations of PV technologies (No. 44-6521a/20/4). C.J.B. gratefully acknowledges financial support through the “Aufbruch Bayern” initiative of the state of Bavaria (EnCN and “Solar Factory of the Future”), the Bavarian Initiative “Solar Technologies go Hybrid” (SolTech), and the German Research Foundation (DFG) SFB 953- No. 182849149 and GRK2495 (ITRG2495).

## Conflict of Interest

The authors declare no conflict of interest.

## Author Contributions

**Vanessa Arango-Marín:** conceptualization (lead); data curation (lead); formal analysis (lead); investigation (lead); methodology (lead); validation (lead); visualization (lead); writing—original draft (lead); writing—review and editing (lead). **Juan S. Rocha-Ortiz:** conceptualization (supporting); data curation (supporting); formal analysis (supporting); investigation (supporting); methodology (supporting); supervision (supporting); validation (supporting); visualization (supporting); writing—original draft (supporting); writing—review and editing (supporting). **Tobias Osterrieder:** data curation (supporting); formal analysis (supporting); investigation (supporting); methodology (supporting); writing—original draft (supporting); writing—review and editing (supporting). **Anastasia Barabash:** investigation (supporting); methodology (supporting); visualization (supporting); writing—original draft (supporting). **Andres Osvet:** writing—original draft (supporting); writing—review and editing (supporting). **Thomas Heumüller:** project administration (supporting); resources (supporting); software (supporting); supervision (supporting); writing—original draft (supporting); writing—review and editing (supporting). **Chao Liu:** supervision (supporting); writing—original draft (supporting); writing—review and editing (supporting). **Jens Hauch:** supervision (lead); writing—original draft (lead); writing—review and editing (lead). **Christoph J. Brabec:** funding acquisition (lead); project administration (lead); resources (lead); supervision (lead); validation (lead); visualization (lead); writing—original draft (supporting); writing—review and editing (supporting). **Jonas Wortmann:** investigation (supporting).

## Data Availability Statement

The data that support the findings of this study are available from the corresponding author upon reasonable request.

## Keywords

aerosol jet printing, organic photovoltaics, ultrasonic spray coating

Received: December 9, 2024  
Published online: January 7, 2025

- [1] P. Maisch, PhD Thesis, *Process Development for Inkjet Printing of Organic Photovoltaics*, Friedrich-Alexander-Universität Erlangen-Nürnberg, Erlangen **2019**.
- [2] N. J. Wilkinson, M. A. A. Smith, R. W. Kay, R. A. Harris, *Int. J. Adv. Manuf. Technol.* **2019**, 105, 4599.
- [3] R. Xia, C. J. Brabec, H. L. Yip, Y. Cao, *Joule* **2019**, 3, 2241.
- [4] W. F. Maier, K. Stowe, S. Sieg, *Angew. Chem., Int. Ed.* **2007**, 46, 6016.
- [5] T. Osterrieder, F. Schmitt, L. Luer, J. Wagner, T. Heumüller, J. Hauch, C. J. Brabec, *Energy Environ. Sci.* **2023**, 16, 3984.
- [6] J. Wagner, C. G. Berger, X. Du, T. Stubhan, J. A. Hauch, C. J. Brabec, *J. Mater. Sci.* **2021**, 56, 16422.
- [7] K. Cheek, E. Neville, K. D'Arezzo, *Optomec. Inc.* **2016**, 260.
- [8] A. Mahajan, C. D. Frisbie, L. F. Francis, *ACS Appl. Mater. Interfaces* **2013**, 5, 4856.
- [9] M. Mette, P. L. Richter, M. Hörteis, S. W. Glunz, *Prog. Photovoltaics: Res. Appl.* **2007**, 15, 621.
- [10] L. Tu, S. Yuan, H. Zhang, P. Wang, X. Cui, J. Wang, Y. Q. Zhan, L. R. Zheng, *J. Appl. Phys.* **2018**, 123, 174905.
- [11] M. K. Hamjah, M. Steinberger, K. C. Tam, H. J. Egelhaaf, C. J. Brabec, J. Franke, in *2021 14th Inter. Congress: Molded Interconnect Devices, MID 2021 – Proc.* **2021**, IEEE, p. 1.
- [12] I. Verboven, J. Silvano, K. Elen, H. Pellaers, B. Ruttens, J. D'Haen, M. K. Van Bael, A. Hardy, W. Deferme, *Adv. Eng. Mater.* **2022**, 24, 2100808.
- [13] K. C. Tam, H. Saito, P. Maisch, K. Forberich, S. Feroze, Y. Hisaeda, C. J. Brabec, H. J. Egelhaaf, *Sol. RRL* **2022**, 6, 2100887.
- [14] S. Ramesh, C. Mahajan, S. Gerdes, A. Gaikewad, P. Rao, D. R. Cormier, I. V. Rivero, *Addit. Manuf.* **2022**, 59, 103090.
- [15] K. C. Tam, P. Kubis, P. Maisch, C. J. Brabec, H. J. Egelhaaf, *Prog. Photovoltaics: Res. Appl.* **2022**, 30, 528.
- [16] A. Wagenpohl, D. Rauh, M. Binder, C. Deibel, V. Dyakonov, *Phys. Rev. B: Condens. Matter Mater. Phys.* **2010**, 82, 115306.
- [17] V. Kalancha, A. These, L. Vogl, I. Levchuk, X. Zhou, M. Barr, M. Bruns, J. Bachmann, S. Virtanen, E. Spiecker, A. Osvet, C. J. Brabec, K. Forberich, *Adv. Electron. Mater.* **2022**, 8, 2100787.
- [18] N. J. Schrenker, Z. Xie, P. Schweizer, M. Moninger, F. Werner, N. Karpstein, M. Mačković, G. D. Spyropoulos, M. Göbel, S. Christiansen, C. J. Brabec, E. Bitzek, E. Spiecker, *ACS Nano* **2021**, 15, 362.
- [19] G. Haacke, *J. Appl. Phys.* **1976**, 47, 4086.
- [20] M. Rother, M. Brohmann, S. Yang, S. B. Grimm, S. P. Schießl, A. Graf, J. Zaumseil, *Adv. Electron. Mater.* **2017**, 3, 1700080.
- [21] C. Yang, E. Zhou, S. Miyanishi, K. Hashimoto, K. Tajima, *ACS Appl. Mater. Interfaces* **2011**, 3, 4053.
- [22] R. Eckstein, G. Hernandez-Sosa, U. Lemmer, N. Mechau, *Org. Electron.* **2014**, 15, 2135.
- [23] A. These, N. H. Khansur, O. Almora, L. Luer, G. J. Matt, U. Eckstein, A. Barabash, A. Osvet, K. G. Webber, C. J. Brabec, *Adv. Electron. Mater.* **2021**, 7, 2001165.
- [24] P. Kopola, B. Zimmermann, A. Filipovic, H. F. Schleiermacher, J. Greulich, S. Rousu, J. Hast, R. Myllylä, U. Würfel, *Sol. Energy Mater. Sol. Cells* **2012**, 107, 252.